LETTER

doi:10.1038/nature11983

Terrestrial water fluxes dominated by transpiration

Scott Jasechko[1], Zachary D. Sharp[1], John J. Gibson[2,3], S. Jean Birks[2,4], Yi Yi[2,3] & Peter J. Fawcett[1]

Renewable fresh water over continents has input from precipitation and losses to the atmosphere through evaporation and transpiration. Global-scale estimates of transpiration from climate models are poorly constrained owing to large uncertainties in stomatal conductance and the lack of catchment-scale measurements required for model calibration, resulting in a range of predictions spanning 20 to 65 per cent of total terrestrial evapotranspiration (14,000 to 41,000 km^3 per year) (refs 1–5). Here we use the distinct isotope effects of transpiration and evaporation to show that transpiration is by far the largest water flux from Earth's continents, representing 80 to 90 per cent of terrestrial evapotranspiration. On the basis of our analysis of a global data set of large lakes and rivers, we conclude that transpiration recycles 62,000 ± 8,000 km^3 of water per year to the atmosphere, using half of all solar energy absorbed by land surfaces in the process. We also calculate CO_2 uptake by terrestrial vegetation by connecting transpiration losses to carbon assimilation using water-use efficiency ratios of plants, and show the global gross primary productivity to be 129 ± 32 gigatonnes of carbon per year, which agrees, within the uncertainty, with previous estimates[6]. The dominance of transpiration water fluxes in continental evapotranspiration suggests that, from the point of view of water resource forecasting, climate model development should prioritize improvements in simulations of biological fluxes rather than physical (evaporation) fluxes.

Unlike river discharges to the oceans[7], the global fluxes of evaporation and transpiration are poorly constrained owing to a lack of methodology to decouple these two water fluxes at the catchment scale. Stable isotope ratios of oxygen ($^{18}O/^{16}O$) and hydrogen ($^{2}H/^{1}H$) in water can be used to separate transpiration from evaporation[8], because the two processes have different effects on these ratios in water. The physical process of evaporation enriches residual water in the heavy isotopes of oxygen and hydrogen, whereas the biological process of transpiration does not produce an isotopic fractionation, assuming an isotopic steady state over annual timescales[8–11]. The pathway water takes after falling as precipitation within a catchment includes mixing, evaporation (fractionation labelled) and transpiration (non-fractionation labelled), until the remaining water accumulates in a downstream lake or river. Each of these catchment processes is ultimately recorded by the isotopic composition of the lake's water. We have compiled a data set of $\delta^{18}O$ and $\delta^{2}H$ values of large lake waters and capitalize on dissimilar isotope effects between evaporation and transpiration to decouple and quantify these two freshwater losses from Earth's surface (isotope content is given by $(R_{sample}/R_{V\text{-}SMOW} - 1) \times 10^3$ ‰, where R is $^{18}O/^{16}O$ for $\delta^{18}O$ and $^{2}H/^{1}H$ for $\delta^{2}H$, and V-SMOW represents standard mean ocean water).

To proceed with this calculation, we first report on the stable oxygen and hydrogen isotope compositions of Earth's large lakes (Fig. 1). The isotopic compositions of lake waters show a broad range in $\delta^{18}O$ and

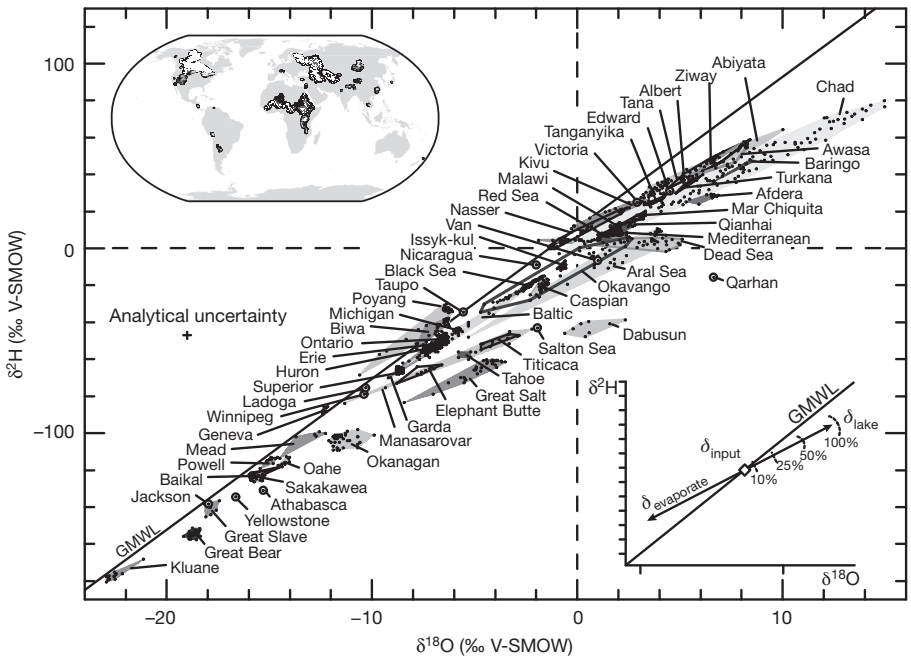

Figure 1 | $\delta^{18}O$ and $\delta^{2}H$ values of large lakes and semi-enclosed seas. The global meteoric water line[12] (GMWL) is shown. The map at top left shows catchment areas covered by the data set. The schematic graph at bottom right shows water inputs to a lake (diamond) and the evaporation trajectory of a lake (percentages refer to evaporation amount).

[1]Department of Earth and Planetary Sciences, University of New Mexico, Albuquerque, New Mexico 87131, USA. [2]Alberta Innovates – Technology Futures, Vancouver Island Technology Park, Victoria, British Columbia V8Z 7X8, Canada. [3]Department of Geography, University of Victoria, Victoria, British Columbia V8W 3R4, Canada. [4]Department of Earth and Environmental Sciences, University of Waterloo, Waterloo, Ontario N2L 3G1, Canada.

δ^2H values: −23‰ to +15‰ and −180‰ to +80‰, respectively. Well-mixed lakes (for example, the North American Great Lakes and Lake Baikal) have relatively homogenous stable isotope compositions, whereas perennially stratified or shallow lakes tend to have greater isotopic variability (for example Lake Kivu and Lake Chad). Headwater lakes located at high latitudes and altitudes (for example, Kluane Lake) have the lowest δ^{18}O and δ^2H values, whereas the closed basin lakes of eastern Africa have the highest δ^{18}O and δ^2H values (for example, Lake Afdera and Lake Turkana). Global lakes do not follow one systematic evaporation trend, reflecting the unique climatology and hydrology of each individual lake catchment. The global meteoric water line plotted in Fig. 1 is a regression of δ^{18}O and δ^2H values of precipitation samples on a global scale[12]. This regression produces a δ^2H/δ^{18}O slope of eight that can be closely reconciled by liquid–vapour isotope effects at chemical equilibrium[13]. However, the disequilibrium process of evaporation results in a strong kinetic isotope effect, with the light isotopologues preferentially partitioned into the vapour phase. This results in δ^2H/δ^{18}O slopes of less than eight, driving the isotope composition of lake waters 'below' the global meteoric water line. Information on the percentage of evaporative losses is retained by the difference between the lake's isotope composition and that of waters entering a basin (δ_{input}; Fig. 1, inset schematic graph). Our global data compilation shows that nearly all lakes fall to the right of the global meteoric water line in δ^{18}O–δ^2H space as a result of evaporation, except in special cases where waters evaporate upwind and re-precipitate in a downwind lake basin (for example Lake Biwa). In what follows, we develop equations describing a stable isotope mass balance of waters within a lake catchment to estimate the percentage of catchment transpiration, and apply these equations to δ^{18}O and δ^2H data for large lake waters.

A lake catchment in hydrologic steady state can be described by a balance between water inputs (I, precipitation and inflows from upstream lakes) and water losses such as precipitation intercepted by vegetation (xP, where x is the fraction of intercepted precipitation for the catchment), open-water and soil evaporation (E), transpiration (T) and liquid losses to rivers or groundwater discharge (Q):

$$I = xP + E + T + Q \quad (1)$$

Similarly, a stable isotope mass balance of a lake catchment is obtained by considering the isotopic composition of each water flux (δ_I, δ_E and so on):

$$\delta_I I = \delta_P xP + \delta_E E + \delta_T T + \delta_Q Q \quad (2)$$

By combining equations (1) and (2), we develop a new equation describing transpiration losses from a catchment:

$$T = \frac{I(\delta_I - \delta_E) - Q(\delta_Q - \delta_E) - xP(\delta_P - \delta_E)}{\delta_T - \delta_E} \quad (3)$$

Each parameter in equation (3) can be estimated from gridded data sets or lake-specific studies, except for the isotope composition of evaporate (δ_E). To calculate δ_E (ref. 14), we use an evaporation model based on laboratory-derived liquid–vapour fractionation factors[13]. The isotope composition of soil and open-water evaporate are grouped into one term (δ_E), and the isotopic composition of transpired moisture (δ_T) is calculated using both shallow and deep-water sources under the assumption that the catchment is in steady state at an annual time step[11] (on average, water molecules spend multiple years within lakes examined here). Physical, isotopic and hydroclimatic data sets for each lake are compiled from available reanalysis and interpolated data[15–18] and are used in equation (3) to calculate catchment transpiration (Methods).

We find that transpiration accounts for more than two-thirds of total surface water evapotranspiration for 85% of the catchments examined (Fig. 2 and Fig. 3a). Remarkably, transpiration also accounts for the majority of evapotranspiration in desert catchments (average, 75%; range, 35% to 95%). *In situ* transpiration measurements in deserts range from 7% to 80% of evapotranspiration[19], in large part because precipitation rates are highest in the headwaters of desert catchments, thereby increasing the importance of these forested ecosystems to the catchment's water balance. Transpiration rates range from less than 100 mm yr^{-1} to approximately 1,300 mm yr^{-1} (Fig. 2 and Supplementary Information, section 1). Our results show that even though open-water evaporation may locally occur at higher rates than transpiration, the fraction of total evapotranspiration represented by evaporation is severely limited by the small areas of open water on Earth's continents (approximately 3%, globally[20]). Therefore, we posit that the biological pump of water into the atmosphere during photosynthetic gas exchange (that is, transpiration), rather than the physical process of evaporation, dominates water losses from the continents. Because plant roots are able to tap into groundwater and soil-water reservoirs, transpiration effectively moves deep sources of water into the atmosphere, whereas evaporation is only effective for water at or near the surface, which explains the very high proportion of transpiration to the overall evapotranspiration flux.

Our results are supported by a cross-plot comparison of isotope-based and conventional open-water evaporation rates ($R^2 = 0.78$ (squared correlation coefficient), slope = 0.92; Supplementary Fig. 1); geographic similarity between compiled *in situ* transpiration measurements[9,10] (of, for example, sap flow) at the forest stand level and our estimates (Fig. 3); and agreement between ^{18}O/^{16}O- and ^{2}H/^{1}H-based evaporation rates using equation (3) ($R^2 = 0.78$, slope = 0.94; Supplementary Figs 2 and 3 and Supplementary Information, section 1). We also note that the time step of our calculated transpiration fluxes ranges from 1 to 1,000 years, averaging 40 years, as dictated by the hydrologic residence time of each lake (Supplementary Table 3). To scale up our calculation to Earth's ice-free land surface, and to provide a fourth check corroborating our catchment transpiration results, we estimate the global transpiration from Earth's landmasses (excluding Antarctica) from a stable isotope mass balance of Earth's entire freshwater reservoir. This estimate is based on the deuterium excess parameter, which includes information contained in both ^{18}O/^{16}O and ^{2}H/^{1}H ($d = \delta^2\text{H} - 8\delta^{18}\text{O}$). We

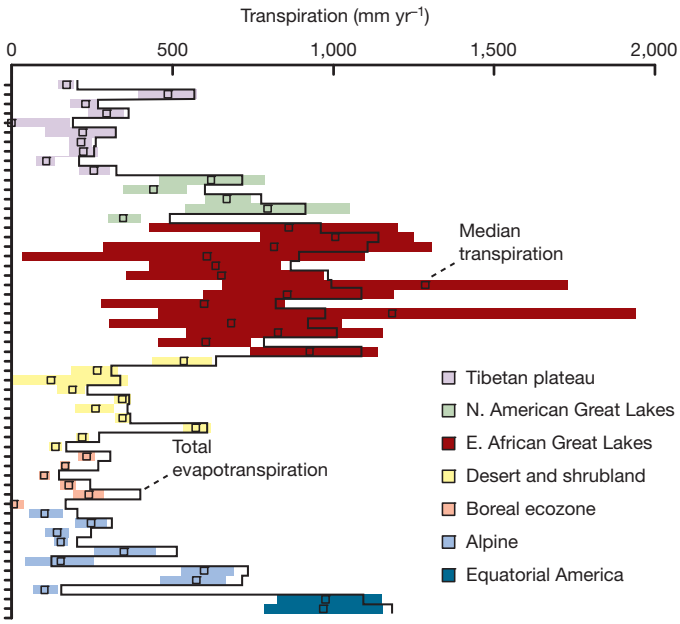

Figure 2 | Transpiration water losses for 56 lake catchments grouped by ecoregion (^{18}O/^{16}O-based results). Each coloured bar represents results for a single lake catchment. Extents of bars show 25th and 75th percentiles of Monte Carlo simulations. Median transpiration (T; square) outputs of Monte Carlo simulations and total evapotranspiration losses (solid line) are shown. The median result is close to the total evapotranspiration for most of the lakes, demonstrating the dominant role of transpiration in total evapotranspiration losses.

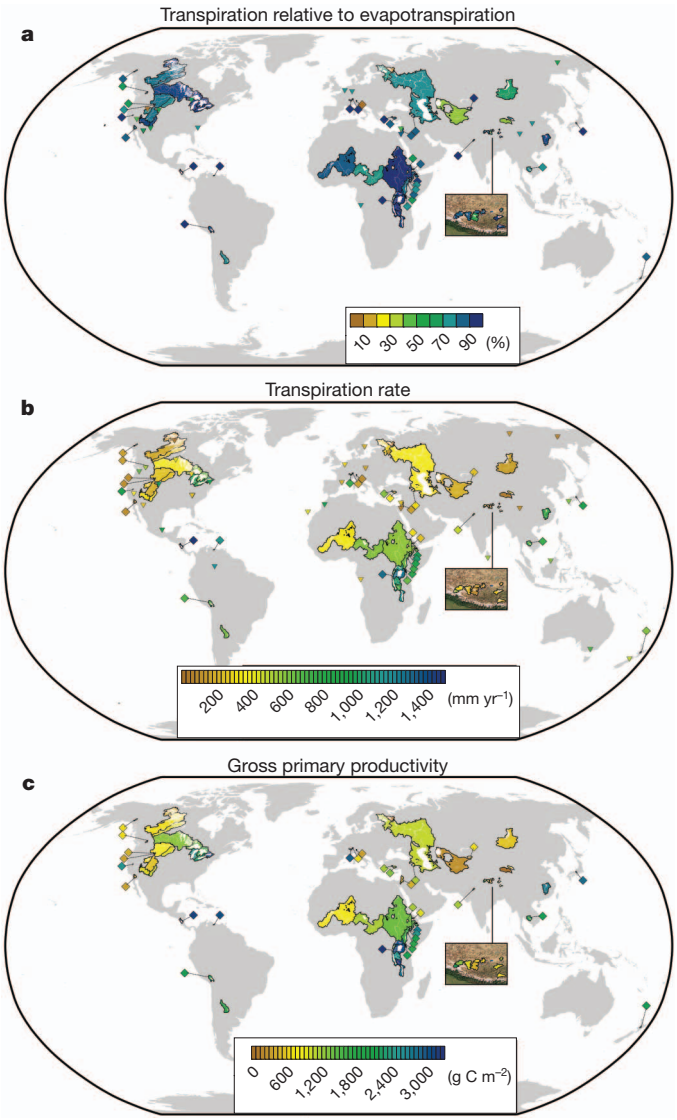

Figure 3 | Transpiration and carbon fluxes within 73 lake catchments. **a**, Transpiration losses as a percentage of total evapotranspiration. **b**, Transpiration rates. **c**, Gross primary productivity for 10% of Earth's continental area. Coloured diamonds are shown for small basins as a visual aid. Inverted triangles represent compiled *in situ* transpiration measurements (for example sap flow[9]).

obtain a similar expression to equation (3) based on the deuterium excess:

$$T = \frac{P(d_P - d_E) - Q(d_Q - d_E) - xP(d_P - d_E)}{d_T - d_E} \quad (4)$$

Terrestrial precipitation ($P = 110{,}000 \pm 10{,}000\,km^3\,yr^{-1}$ (ref. 17), $d_P = 9.5 \pm 1‰$ (ref. 12)) is the only input of water to the continents, and water is lost through river discharges to the oceans ($Q = 37{,}300 \pm 700\,km^3\,yr^{-1}$ (ref. 7), $d_Q = 6.8 \pm 3.8‰$; Supplementary Information, section 2), terrestrial evaporation ($d_E = 75 \pm 30‰$ (this work)), transpiration ($d_T = 8 \pm 3‰$) or interception by vegetation ($xP = 7{,}500 \pm 1{,}500\,km^3\,yr^{-1}$ (refs 16, 17), $d_P = 9.5 \pm 1‰$ (ref. 12)). Solving equation (4) shows that transpiration accounts for 80% to 90% of terrestrial evapotranspiration (respectively the 25th and 75th percentiles of a Monte Carlo sensitivity analysis). Volumetrically, transpiration converts $62{,}000 \pm 8{,}000\,km^3\,yr^{-1}$ of liquid water into atmospheric vapour, requiring $33 \pm 4\,W\,m^{-2}$ of latent heat, or roughly half of all solar energy absorbed by the continents[21] (approximately $70\,W\,m^{-2}$). Results show that 90% of precipitation falling on land[18] ($111{,}000\,km^3\,yr^{-1}$) is already appropriated to ecosystems for either primary production ($62{,}000 \pm 8{,}000\,km^3\,yr^{-1}$) or as aquatic habitat in rivers[7] ($37{,}000\,km^3\,yr^{-1}$), an important consideration for diversion of in-stream flows.

We can use our transpiration fluxes to calculate carbon assimilation by terrestrial vegetation by linking the water and carbon cycles[22]. The molar ratio of CO_2 assimilated during photosynthesis to transpired H_2O is known as water-use efficiency (WUE) and is dependent on a variety of factors including the type of photosynthetic pathway used by a particular plant species (C_3, C_4 or CAM) and atmospheric conditions such as vapour pressure deficit and CO_2 concentration[23]. We compile WUE data and couple these to atmospheric vapour pressure deficits and C_3–C_4 vegetation abundances to develop global grids of WUE (Methods). Catchment transpiration fluxes and gridded WUEs are applied to calculate gross primary production within each catchment (Fig. 3c). On the global scale, we weight our global grids of WUE according to vegetation density and calculate the global WUE of the terrestrial biosphere to be 3.2 ± 0.9 mmol CO_2 per mol H_2O. Applying this ratio to our global transpiration flux ($62{,}000 \pm 8{,}000\,km^3\,yr^{-1}$ of H_2O), we calculate gross primary production to be $129 \pm 32\,GtC\,yr^{-1}$. This flux is consistent with a recent estimate of $123 \pm 8\,GtC\,yr^{-1}$ (ref. 6) and provides a fifth line of support for the large transpiration fluxes reported in our work.

Linkages made here between the water and carbon cycles highlight a new stable-isotope-based methodology that can be used to monitor and map ongoing changes to Earth's water cycle[24,25] as well as modifications to carbon assimilation rates under increased atmospheric temperatures and CO_2 concentrations. Our results show that the water and carbon cycles are linked in such a way that transpiration must account for more than 80% of continental evapotranspiration to maintain a mass balance between these two biogeochemical fluxes (plant transzpiration and CO_2 uptake). Given the importance of transpiration, it follows that the physiological response of vegetation to a warmer and CO_2-enriched atmosphere will have a dominant effect on future changes to evapotranspiration and the terrestrial hydrological cycle. Furthermore, changes in natural ecosystems via land-use modifications or climate changes will have notable effects on river discharges and, consequently, fluvial sediment loads, chemical weathering on continents, and atmospheric latent heat transport.

Climate change is expected to affect global transpiration[3]. Considering the dominance of transpiration in continental evapotranspiration shown here, future changes in global transpiration will affect land temperatures by altering latent heat fluxes from continents, and will also change the fraction of precipitation entering rivers. Our catchment-scale results can be applied as a calibration tool for climate models, which should shift the prevailing focus on physical climate data towards ecosystem water requirements and so result in better predictions of continental evapotranspiration and water recycling in a warmer future climate.

METHODS SUMMARY

In equation (3), hydrologic inputs (I) include precipitation[17] and upstream lake inflows. Catchment losses include interception (xP; ref. 16), liquid outflows (Q; lake-specific data), evaporation (E) and transpiration (T). The isotopic composition of precipitation (δ_P) is computed from monthly grids[15] weighted spatially (grid cell, i) and temporally (month, j) to precipitation distribution as follows:

$$\delta_P = \frac{1}{\sum_{i=1}^{n} P_i} \sum_{i=1}^{n} \left(\frac{\sum_{j=1}^{12} P_j \delta_{P_j}}{\sum_{j=1}^{12} P_j} \right)_i P_i \quad (5)$$

For chain lakes, inflows from an upstream lake are included in the calculation of δ_I. For lakes not in equilibrium with current climate, δ_I is calculated from the intercept between a computed evaporation trend[26] and the global meteoric water line[12]. The isotopic composition of lake water is used to estimate that of liquid outflows (that is, $\delta_Q = \delta_{lake}$). The isotopic composition of transpired moisture (δ_T) is estimated by weighting the isotopic composition of precipitation[15] spatially (i) to

mean long-term normalized difference vegetation indices (NDVI; proxy for vegetation density). A range of two temporal (j) weighting approaches[10] is used for δ_T, one weighted to growing season (NDVI values (equation (5)) and another to monthly precipitation (equation (6)):

$$\delta_{T\text{-SHALLOW}} = \frac{1}{\sum_{i=1}^{n}\mathrm{NDVI}_i}\sum_{i=1}^{n}\left(\frac{\sum_{j=1}^{12}\mathrm{NDVI}_j\delta_{P_j}}{\sum_{j=1}^{12}\mathrm{NDVI}_j}\right)_i \mathrm{NDVI}_i \quad (6)$$

$$\delta_{T-\mathrm{DEEP}} = \frac{1}{\sum_{i=1}^{n}\mathrm{NDVI}_i}\sum_{i=1}^{n}\left(\frac{\sum_{j=1}^{12}P_j\delta_{P_j}}{\sum_{j=1}^{12}P_j}\right)_i \mathrm{NDVI}_i \quad (7)$$

Finally, the isotopic composition of evaporate is computed using an evaporation model[14]:

$$\delta_E = \frac{(\delta_{\mathrm{lake}} - \varepsilon^*)/\alpha^* - h\delta_{\mathrm{A}} - \varepsilon_{\mathrm{K}}}{1 - h + \varepsilon_{\mathrm{K}}} \quad (8)$$

This takes into account temperature-dependent[17] equilibrium[13] (α^*; $\varepsilon^* = \alpha^* - 1$) and humidity-dependent[17] (h) kinetic (ε_{K}; ref. 27) fractionation factors normalized to lake temperatures[28]. The isotopic composition of atmospheric vapour (δ_{A}) is computed on the basis of a precipitation-equilibrium assumption[13,15,17,26] and by using isotope-enabled climate model grids[18]. Humidity, temperature and δ_{A} are each weighted to the monthly evaporation amount. A Monte Carlo simulation is used to assess calculation uncertainty embedded in each input parameter (Supplementary Information, sections 3 and 4). Plant water-use efficiency is calculated by applying growing-season daytime vapour pressure deficit[17,29] (VPD) to C_3 ($\mathrm{WUE_{C3}} = 4.21(\mathrm{VPD})^{-0.67}$ mmol CO_2 per mol H_2O) and C_4 ($\mathrm{WUE_{C4}} = 6.91(\mathrm{VPD})^{-0.40}$ mmol CO_2 per mol H_2O) vegetation abundances[30].

Full Methods and any associated references are available in the online version of the paper.

Received 6 September 2012; accepted 4 February 2013.
Published online 3 April 2013.

1. Lawrence, D. M., Thornton, P. E., Oleson, K. W. & Bonan, G. B. Partitioning of evaporation into transpiration, soil evaporation, and canopy evaporation in a GCM: impacts on land-atmosphere interaction. *J. Hydrometeorol.* **8,** 862–880 (2007).
2. Alton, P., Fisher, R., Los, S. & Williams, M. Simulations of global evapotranspiration using semiempirical and mechanistic schemes of plant hydrology. *Glob. Biogeochem. Cycles* **23,** GB4023 (2009).
3. Cao, L., Bala, G., Caldeira, K., Nemani, R. & Ban-Weiss, G. Importance of carbon dioxide physiological forcing to future climate change. *Proc. Natl Acad. Sci. USA* **107,** 9513–9518 (2010).
4. Ito, A. & Motoko, I. Water-use efficiency of the terrestrial biosphere: a model analysis focusing on interactions between the global carbon and water cycles. *J. Hydrometeorol.* **13,** 681–694 (2012).
5. Gerten, D. *et al.* Contemporary ''green'' water flows: simulations with a dynamic global vegetation and water balance model. *Phys. Chem. Earth* **30,** 334–338 (2005).
6. Beer, C. *et al.* Terrestrial gross carbon dioxide uptake: global distribution and covariation with climate. *Science* **329,** 834–838 (2010).
7. Dai, A. & Trenberth, K. E. Estimates of freshwater discharge from continents: latitudinal and seasonal variations. *J. Hydrometeorol.* **3,** 660–687 (2002).
8. Yakir, D. & Wang, X. F. Fluxes of CO_2 and water between terrestrial vegetation and the atmosphere estimated from isotope measurements. *Nature* **380,** 515–517 (1996).
9. Williams, D. *et al.* Evapotranspiration components determined by stable isotope, sap flow and eddy covariance techniques. *Agric. For. Meteorol.* **125,** 241–258 (2004).
10. Dawson, T. E. Determining water use by trees and forests from isotopic, energy balance and transpiration analyses: the roles of tree size and hydraulic lift. *Tree Physiol.* **16,** 263–272 (1996).
11. Welp, L. R. *et al.* $\delta^{18}O$ of water vapor, evapotranspiration and the sites of leaf water evaporation in a soybean canopy. *Plant Cell Environ.* **31,** 1214–1228 (2008).
12. Rozanski, K., Araguas-Araguas, L. & Gonfiantini, R. in *Climate Change in Continental Isotopic Records* (eds Swart, P. K. *et al.*) 1–36 (Am. Geophys. Union, 1993).
13. Horita, J. & Wesolowski, D. Liquid-vapour fractionation of oxygen and hydrogen isotopes of water from the freezing to the critical temperature. *Geochim. Cosmochim. Acta* **58,** 3425–3437 (1994).
14. Craig, H. & Gordon, L. I. in *Stable Isotopes in Oceanographic Studies and Paleotemperatures* (ed. Tongiorgi, E.) 9–130 (Lab. Geol. Nucl., 1965).
15. Bowen, G. J. & Revenaugh, J. Interpolating the isotopic composition of modern meteoric precipitation. *Wat. Resour. Res.* **39,** 1299 (2003).
16. Miralles, D. G., Gash, J. H., Holmes, T. R. H., de Jeu, R. A. M. & Dolman, A. J. Global canopy interception from satellite observations. *J. Geophys. Res.* **115,** D16122 (2010).
17. New, M., Lister, D., Hulme, M. & Makin, I. A high-resolution data set of surface climate over global land areas. *Clim. Res.* **21,** 1–25 (2002).
18. Yoshimura, K., Kanamitsu, M., Noone, D. & Oki, T. Historical isotope simulation using reanalysis atmospheric data. *J. Geophys. Res.* **113,** D19108 (2008).
19. Reynolds, J. F., Kemp, P. R. & Tenhunen, J. D. Effects of long-term rainfall variability on evapotranspiration and soil water distribution in the Chihuahuan desert: a modeling analysis. *Plant Ecol.* **150,** 145–159 (2000).
20. Downing, J. A. *et al.* The global abundance and size distribution of lakes, ponds, and impoundments. *Limnol. Oceanogr.* **51,** 2388–2397 (2006).
21. Trenberth, K. E., Fasullo, J. T. & Kiehl, J. Earth's global energy budget. *Bull. Am. Meteorol. Soc.* **90,** 311–323 (2009).
22. Beer, C., Reichstein, M., Ciais, P., Farquhar, G. D. & Papale, D. Mean annual GPP of Europe derived from its water balance. *Geophys. Res. Lett.* **34,** L05401 (2007).
23. Farquhar, G. D., Ehleringer, J. R. & Hubick, K. T. Carbon isotope discrimination and photosynthesis. *Annu. Rev. Plant Physiol. Plant Mol. Biol.* **40,** 503–537 (1989).
24. Jung, M. *et al.* Recent decline in the global land evapotranspiration trend due to limited moisture supply. *Nature* **467,** 951–954 (2010).
25. Durack, P. J., Wijffels, S. E. & Matear, R. J. Ocean salinities reveal strong global water cycle intensification during 1950 to 2000. *Science* **336,** 455–458 (2012).
26. Gibson, J. J., Birks, S. J. & Edwards, T. W. D. Global prediction of δ_A and δ^2H-$\delta^{18}O$ evaporation slopes for lakes and soil water accounting for seasonality. *Glob. Biogeochem. Cycles* **22,** GB2031 (2008).
27. Gonfiantini, R. in *Handbook of Environmental Isotope Geochemistry* Vol. 2: *The Terrestrial Environment* (eds Fritz, P. & Fontes, J.-Ch.) 113–163 (Elsevier, 1986).
28. Buck, A. L. New equations for computing vapour pressure and enhancement factor. *J. Appl. Meteorol.* **20,** 1527–1532 (1981).
29. Hijmans, R. J., Cameron, S. E., Parra, J. L., Jones, P. G. & Jarvis, A. Very high resolution interpolated climate surfaces for global land areas. *Int. J. Climatol.* **25,** 1965–1978 (2005).
30. Global Energy and Water Cycle Experiment. International Satellite Land-Surface Climatology Project. http://www.gewex.org/islscpdata.htm (2012).

Supplementary Information is available in the online version of the paper.

Acknowledgements We thank T. W. D. Edwards, T. Gleeson and M. C. Molles Jr for comments on the manuscript, and are grateful to O. Kwiecien, D. G. Miralles, B. K. Nyarko, K. Yoshimura and F. Yuan for providing access to isotope and gridded data sets. Support for this work was provided by a graduate fellowship awarded to S.J. by the Caswell Silver Foundation through the University of New Mexico.

Author Contributions S.J. designed the study, compiled each data set, did the geographic information system and remote sensing work, developed the equations, did the water balance and carbon flux calculations, and wrote the paper. Z.D.S., J.J.G., S.J.B., Y.Y. and P.J.F. discussed the results, commented on the manuscript and contributed to text.

Author Information Reprints and permissions information is available at www.nature.com/reprints. The authors declare no competing financial interests. Readers are welcome to comment on the online version of the paper. Correspondence and requests for materials should be addressed to S.J. (jasechko@unm.edu).

METHODS

For each basin, eight input terms are required for calculation of transpiration losses using equation (3): I, Q, x, δ_Q, δ_I, δ_T, δ_P and δ_E. Water inputs (I) include precipitation and upstream lake inflows. Precipitation inputs are obtained from high-resolution physical climate grids[17]. Upstream chain lake inflows are retrieved from lake-specific sources, as are liquid outflows (Q) for each lake. The proportion of incident precipitation that is intercepted and returned to the atmosphere (x) is obtained from satellite-based gridded data[16]. The isotope composition of liquid outflows (δ_Q) from each lake is obtained from epilimnion $\delta^{18}O$ and δ^2H values for samples nearest to a lake's outflow ($\delta_{lake} = \delta_Q$). The isotope composition of precipitation entering a basin is calculated by weighting spatially (grid cell, i) and temporally (month, j) to monthly precipitation amount (P) as follows:

$$\delta_P = \frac{1}{\sum_{i=1}^{n} P_i} \sum_{i=1}^{n} \left(\frac{\sum_{j=1}^{12} P_j \delta_{P_j}}{\sum_{j=1}^{12} P_j} \right)_i P_i \quad (5)$$

Monthly δ_P estimates[15] and monthly precipitation amounts are obtained from gridded data sets. For headwater lakes, precipitation is the sole input (that is, $I = P$ and $\delta_I = \delta_P$); for chain lakes, δ_P is flux-weighted against the isotopic composition of riverine inputs entering the catchment from upstream chain lakes. Large lakes with residence times longer than approximately 300 years (for example, Lake Baikal) are in an isotopic disequilibrium with current climate. For these lakes, a $\delta^2H/\delta^{18}O$ evaporation slope is calculated[26] using the lake isotope data. The intercept of the resulting 'evaporation line' with the global meteoric water line[12] is applied as a mean 'long-term' estimate of δ_I. This approach is also applied to headwater lakes where grids produce unrealistic δ_I estimates ($\delta_I > \delta_{lake}$). Lakes with an outflow that periodically reverses flow (Tonlé Sap and Poyang Lake) or mixes with a geographically separate lake (Lake Michigan and Lake Huron) are treated specially, and the isotopic composition and flux of return flows are included in the computation of δ_I.

The isotopic composition of transpired moisture is calculated using an average of two approaches (both based on similar δ_P grids[15]), the first representing the isotope composition of shallow waters during the growing season and the second estimating the annual isotope composition of recharge. Plants tapping shallow water sources draw on precipitation falling during the growing season, whereas deep-rooted vegetation transpires ground waters that more closely represent the recharge-weighted isotope composition of precipitation[10].

To estimate the isotope composition of transpired moisture (δ_T) for shallow 'growing season' waters, the isotope composition of precipitation (δ_P) is weighted to a proxy for chlorophyll abundance using long-term monthly mean values of normalized difference vegetation indices (NDVI; equation (5)). Monthly NDVI values less than zero were assigned a value of zero, because these cells host minor amounts of photosynthetic activity:

$$\delta_{T-SHALLOW} = \frac{1}{\sum_{i=1}^{n} NDVI_i} \sum_{i=1}^{n} \left(\frac{\sum_{j=1}^{12} NDVI_j \delta_{P_j}}{\sum_{j=1}^{12} NDVI_j} \right)_i NDVI_i \quad (6)$$

To estimate the isotope composition of transpired moisture from vegetation with deep roots, we weight the isotope composition of precipitation temporally to monthly precipitation amount, and then consider the spatial distribution of vegetation by applying long-term annual average NDVI indices:

$$\delta_{T-DEEP} = \frac{1}{\sum_{i=1}^{n} NDVI_i} \sum_{i=1}^{n} \left(\frac{\sum_{j=1}^{12} P_j \delta_{P_j}}{\sum_{j=1}^{12} P_j} \right)_i NDVI_i \quad (7)$$

The range of values from the two approaches is used to estimate δ_T (see Supplementary Information, section 3 for treatment of uncertainty in each input parameter).

The isotope composition of evaporated moisture is estimated using an evaporation model developed to calculate the isotopic composition of evaporate[14]:

$$\delta_E = \frac{(\delta_{lake} - \varepsilon^*)/\alpha^* - h\delta_A - \varepsilon_K}{1 - h + \varepsilon_K} \quad (8)$$

where δ_{lake} is the isotope composition of each lake, α^* is the temperature-dependent[17] equilibrium liquid–vapour fractionation factor[13] (with $\varepsilon^* = \alpha^* - 1$), h is the relative humidity[17] normalized to surface water temperatures and $\varepsilon_K = C_K(1 - h)$ is a kinetic separation factor with C_K representing resistance ratios for various stable water isotopologues ($C_K = 14.2$ for the $\delta^{18}O$ model and $C_K = 12.5$ for the δ^2H model[27]).

To calculate δ_E, four inputs are required: atmospheric specific humidity, lake water temperature (T_L), air temperature (T_A) and the isotopic composition of atmospheric moisture (δ_A). Specific humidity values are calculated[28] using long-term monthly mean temperature and relative humidity grids[17] (h_A), lake surface temperatures are used to calculate monthly saturation vapour pressures, and then relative humidity is computed using the specific humidity and computed saturation vapour pressure. The isotope composition of atmospheric water vapour (δ_A) is obtained in two ways. First, the isotope composition of atmospheric moisture can be estimated by assuming that the isotope composition of precipitation reflects the isotopic atmospheric vapour offset by equilibrium isotope effects[26] (calculated with monthly gridded δ_P values[15] and air temperatures[17], applied to liquid–vapour equilibrium fractionation factors[13]). Alternatively, values for δ_A are derived from long-term monthly average outputs from an isotope-enabled global climate model (IsoGSM[18]). An average δ_A value is taken from the two approaches and used as a first estimate (Supplementary Information, section 3). Finally, atmospheric vapour $\delta^{18}O$ and δ^2H values, humidity, and lake and air temperatures are weighted temporally to monthly evaporation amount for each lake. This is a crucial step for lakes that experience large seasonal variations in evaporation fluxes. Uncertainty in each input parameter is assessed by a Monte Carlo analysis (Supplementary Information, sections 3 and 4). Plant-scale water-use efficiency grids are developed for Earth from a compilation of data sets (Supplementary Table 6 and Supplementary Figs 5 and 6). Daytime vapour pressure deficit (VPD) is calculated at a monthly time step using humidity[17] and daytime temperature (maximum daily temperature minus average daily temperature[29]), and is weighted to growing season via NDVI indices. These growing-season daytime vapour pressure deficits are input into VPD–WUE regressions from compiled data for C_3 ($WUE_{C3} = 4.21(VPD)^{-0.67}$ mmol CO_2 per mol H_2O) and C_4 ($WUE_{C4} = 6.91(VPD)^{-0.40}$ mmol CO_2 per mol H_2O) vegetation, and the respective proportions of C_3 and C_4 plants within each grid cell[30] are applied to develop WUE grids for Earth. WUE grids are applied to catchment transpiration fluxes to calculate gross primary production within each lake basin.